We are IntechOpen, the world's leading publisher of Open Access books Built by scientists, for scientists

4,800
Open access books available

122,000
International authors and editors

135M
Downloads

Our authors are among the

154
Countries delivered to

TOP 1%
most cited scientists

12.2%
Contributors from top 500 universities

CLARIVATE ANALYTICS BOOK CITATION INDEX INDEXED

WEB OF SCIENCE™

Selection of our books indexed in the Book Citation Index in Web of Science™ Core Collection (BKCI)

Interested in publishing with us?
Contact book.department@intechopen.com

Numbers displayed above are based on latest data collected.
For more information visit www.intechopen.com

3

Mine-suspected Area Reduction Using Aerial and Satellite Images

Acheroy Marc and Yvinec Yann
Royal Military School
Belgium

1. Introduction

A huge amount of antipersonnel (AP) mines is polluting the environment in at least 84 countries (ICBL, 2005). Thanks to the Mine Ban Treaty, also known as the Ottawa Convention, mine clearing operations have been organized in a more controlled and effective way. Nevertheless, mine clearance remains a very slow and resource demanding process. On average, a mine-clearance expert clears an area of 10m² every working day with conventional tools, i.e. metal detectors and prodders. Five years were needed to clear only 146km² in Cambodia, which gives an idea of the large scale of the problem (ICBL, 2005). Therefore, humanitarian mine clearance operations must be understood and designed correctly, with the conviction that their main goal is to provide efficient aid to innocent people, who may be severely injured by this dreadful pollution. In this context, it is important to keep in mind the recommendations made during the Standing Committee on Mine Clearance, Mine Risk Education and Mine Action Technologies. These recommendations clearly state that (i) technologists should avoid building technologies based on assumed needs and should work interactively with end-users, (ii) appropriate technologies could save human lives and increase mine action efficiency and (iii) nothing is more important than understanding the working environment (Acheroy, 2003; JMU, 2007).
The analysis of current mine clearance campaigns not only reveals the far too long time needed to clear polluted terrain, but also brings to the fore a far too large false alarm rate, the threat of plastic mines, difficult to detect by classical means such as metal detectors, and the large variety of mine clearance scenarios, depending on the country, the region, the climate and the place of pollution (houses in villages, roads, agricultural fields, etc). This tends to make mine detection a very complex problem for which no silver bullet solution exists. Further, the concept of mine action itself is evolving. Indeed, as most of the time mine detection and removal are still done manually and as there is still a huge amount of contaminated areas, obviously, it will be impossible to reach a mine-free world at the horizon 2010 as required by the Mine Ban Treaty (GICHD, 2007). Consequently, the first priority of mine action becomes to allow affected countries, regions and people to reach a normal way of life according to local socio-economic standards. This new vision tends to increase the importance and the development of management tools facilitating prioritisation and contributing to a rational and efficient distribution of the resources available. Danger

Source: Humanitarian Demining: Innovative Solutions and the Challenges of Technology, Book edited by: Maki K. Habib, ISBN 978-3-902613-11-0, pp. 392, February 2008, I-Tech Education and Publishing, Vienna, Austria

and risk assessment maps provided by the SMART[1] project described in this Chapter, are possible entries of such management systems.
This Chapter is subdivided in 11 Sections. Sections 2 and 3 discuss the problem of close-in detection and area reduction, and sketch the SMART approach as a tentative to solve the problem of mine-suspected area reduction. Sections 4 to 11 describe the SMART processing tools. Section 4 presents the available data. Section 5 introduces the image-processing concept. Section 6 summarizes the pre-processing algorithms. Section 7 sketches the anomaly detection tools. Section 8 describes feature extraction methods. Section 9 summarizes the classification algorithms, while Section 10 and 11 address the change detection and data fusion approaches respectively.

2. The Problem of Mine-suspected Area Reduction

In order to understand the incurred risks, let us consider the event A : "*occurrence of an alarm*'' in a given position $\mathbf{x} = (x, y)$ (obviously depending on the field reality but also on the detection system in use) and two contradictory events M : "*the presence of mines*'' and $\overline{M}$ "*the absence of mine*''. The probability $p_A(\mathbf{x})$ of the occurrence of an alarm in $\mathbf{x} = (x, y)$ can be expressed as follows:

$$p_A(\mathbf{x}) = p_M(\mathbf{x}).p_{A/M}(\mathbf{x}) + p_{\overline{M}}(\mathbf{x}).p_{A/\overline{M}}(\mathbf{x}) \quad (1)$$

Therefore, the important parameters characterizing the mine detection problem, are the mine occurrence probability, the detection probability and the false alarm probability (Acheroy, 2007):

- The *mine occurrence probability* in a given position $\mathbf{x}$ of a minefield, $p_M(\mathbf{x}) = 1 - p_{\overline{M}}(\mathbf{x})$, expresses the local mine density of that minefield. Obviously, it is impossible to control this parameter which depends on the field reality. Nevertheless, this parameter is very important for assessing the probability of an alarm in a given location $\mathbf{x}$ of the minefield.
- The *detection probability*, $p_{A/M}(\mathbf{x})$, is the probability of having an alarm in a given position $\mathbf{x}$ of a minefield for a given sensor system, if there is at least one mine in that position. This probability gives an indirect measure of the non-detection probability of that sensor system as well.
- The *probability of false alarm*, $p_{A/\overline{M}}(\mathbf{x})$, also called *false alarm rate*, is the probability of having an alarm, for a given sensor system, in a given location $\mathbf{x}$ if there is no mine in that location.

The two latter definitions are extremely important to understand the mine action problem and to design mine clearance systems. Note that a more precise expression for (1) should in particular take into account a sensor sensitivity area around the mine, but this is out of the scope of this Chapter. Obviously, the detection probability $p_{A/M}(\mathbf{x})$ should be as close as possible to one. Evaluating the detection probability also amounts to evaluate the risk

[1] "Space and airborne Mined Area Reduction Tools" (SMART), project funded in the 6th framework program by the European Commission / DG / INSO

$p_{\overline{A}/M}(\mathbf{x})$ of the occurrence of a mine that is not detected, since $p_{\overline{A}/M}(\mathbf{x}) = 1 - p_{A/M}(\mathbf{x})$. This risk is concerned with human safety and is therefore of the utmost importance. No such risk is acceptable and it is therefore an absolute requirement that a mine clearance system should decrease the probability of such a risk to the lowest upper bound possible. Therefore, any mine clearance operation enhancement must result in the highest possible detection probability $p_{A/M}(\mathbf{x})$ (close to one) and in the smallest possible false alarm rate $p_{A/\overline{M}}(\mathbf{x})$, all that at the lowest price. Unfortunately, increasing the detection probability generally results in increasing the false alarm rate. The most efficient way for increasing the detection probability while minimizing the false alarm rate consists in using several complementary sensors in parallel and in fusing the information collected by these sensors (Milisavljević &Bloch, 2002). The problem of sensor fusion is discussed in more detail in Chapter 4.

Let us now discuss the problem of mine-suspected area reduction. This important challenge consists of finding *where the mines are not*. Mine-suspected area reduction, recognized by the mine action community as a mine action activity at least as crucial as close-in detection, enables to reduce mine clearance time and resources.

Mine-suspected area reduction means finding the set of positions **x** for which $p_M(\mathbf{x})$ equals zero. Under this condition, Equation (1) yields

$$p_A(\mathbf{x}) = p_{A/\overline{M}}(\mathbf{x}) \tag{2}$$

and mine-suspected area reduction with classical tools (e.g. metal detectors) is affected by the high false alarm rate ($p_{A/\overline{M}}(\mathbf{x})$) of current sensors, making, as said earlier, the corresponding operations slow, tedious and resource demanding. Further, long-term empirical data from the Croatian Mine Action Centre (CROMAC) show that around 10% to 15% of the suspected area in Croatia is actually mined (SMART, 2003). The minefield records alone, beyond the fact they are not always reliable and complete, do not contain enough information for the proper allocation of limited mine clearance resources to really mined areas. Decision makers need additional information.

This means that a broader approach is needed, which has to include *a priori* knowledge. Indeed, if no *a priori* knowledge is available about context as conflict history, strategies and tactics of the parties, communication networks, terrain configuration, power lines, land use, etc., the *a priori* probability of having a mine in a given location $p_M(\mathbf{x})$ is distributed uniformly in **x** and the only method to clear of mines is the classical close-in detection. If on the contrary *a priori* information is available on the distribution of $p_M(\mathbf{x})$, especially by deducing from the context where the mines are certainly not (e.g. agricultural fields in use) and where the mines are possibly present (e.g. along the confrontation lines, in the vicinity of trenches, on tops of hills that are possible artillery positions, etc.), it makes sense to build a risk map ($p_{M/context}(\mathbf{x})$) of the affected areas. This assumes to define a list of indicators of mine presence ($p_{M/context}(\mathbf{x})$ is not negligible) and absence ($p_{M/context}(\mathbf{x})$ is close to zero) as well as a list of tools and methods to detect them. One of the most appropriate methods to build a risk map is associating airborne and satellite data, with context and ground truth data collected during field campaigns. Analysing the collected data with modern remote sensing tools, as land use classification, anomaly detection and change detection, considered as experts, and fusing their "opinions" enables to produce the so-called risk or danger maps. The main advantage of airborne methods rests in the possibility to reduce areas located in

regions that cannot be accessed without very costly safe lanes and full safety procedures that are mandatory when entering the minefields. Further, the assessment of areas for reduction and assessment of spatial danger distribution can be performed in short time over large areas.
In the context of mine action, a frequently asked question concerns the possibility of directly detecting mines using high-resolution airborne sensors. As part of their policy to assist Developing Countries, the European Commission (the former DG-VIII) and the participating member states have funded in 1997 a "Pilot project on airborne minefield detection in Mozambique" which has clearly shown that it is impossible to find antipersonnel landmines even with a very high-resolution (order of magnitude of a few millimetres) airborne sensors neither using objective signal processing tools nor using subjective photo-interpretation (Druyts et al, 1998).

3. The SMART Approach

There are different well-known methods in use to perform mine-suspected area reduction, especially mechanical ones. Nevertheless, most of the time these methods are changing (very often damaging) the environment and the ecosystem, and are expensive. Therefore, several approaches have been developed, trying, when possible, to acquire the necessary information remotely from space or air. In those cases, the information is collected using appropriate sensors, associated with context information collected from the field, and integrated in a geographical information system. Different projects have been initiated in this context (ARC, MINESEEKER, etc., see EUDEM2 website (EUDEM, 2007), for more information). This chapter is intentionally limited to the description of SMART, one of the most promising projects on this matter, applied to Croatia.
The goal of SMART is to provide the human analyst with a GIS-based system – the SMART system – augmented with tools and methods specifically dedicated to SAR and multi-spectral data processing in order to assist him in his interpretation of the mine-suspected scenes, during the area reduction process. The advantages of such tools and methods rest in the possibility to process automatically a large amount of data and to summarize and visualize large amounts of information (SMART, 2004). The use of SMART includes a field survey and an archive analysis in order to collect knowledge about the site, a satellite data collection, a flight campaign to record the data, – multi-spectral with the Daedalus sensor and polarimetric SAR with the E-SAR from DLR[2] –, and the exploitation of the SMART tools by an operator to detect indicators of presence or absence of mine-suspected areas. A data fusion module based on belief functions and fuzzy sets helps the operator to prepare thematic maps that synthesize all the knowledge gathered with these indicators. These maps of indicators, transformed into *risk maps* designed to help the area reduction process, show how dangerous an area may be according to the location of known indicators and into *priority maps* indicating which areas to clear first, accounting for socio-economic impact and political priorities. Figure 1. presents an example of a risk map. Table 1. presents a summary of the results obtained with SMART and shows a global substantial area reduction rate of 25% and a misclassification rate of 0.1% for what SMART considers as not mined and is actually mined. Further, it must be noted first, that the reduction rate strongly varies from

[2] DLR: Deutsches Zentrum für Luft- und Raumfahrt

one test site to another (from 10 to 50%), but that the error rate remains relatively constant, second, that the marginal errors (0.1%) lie at the frontier of contaminated areas.

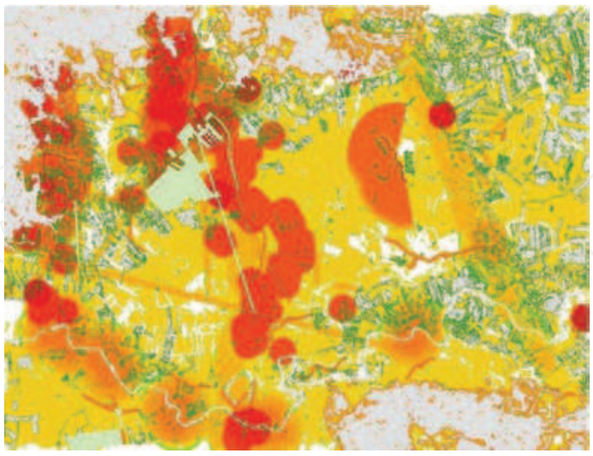

Fig. 1. : Continuous 'risk map' - the scale of risk ranges from red (danger) to green (no danger), white means no status (forests) - Source: ULB

Test site	Area subject to validation (km^2)	Area proposed for reduction (km^2)	Reduction rate (%)	Error rate (%)
Total	3.9	0.98	25	0.1

Table 1. Global results obtained by SMART

4. Available Data

The available data include SAR, multi-spectral, high resolution optical and satellite data. SAR data were collected with the ESAR system of DLR in vv-polarization (waves are vertically transmitted and received) X- and C-band, and in fully polarimetric (hh, hv, vv, vh-polarizations) L- and P-band. Table 2., where SLC stands for Single Look Complex and ML for Multilook, summarizes the characteristics of these SAR data. SAR and multi-spectral data have been geo-coded.

Bandes	**Polarisation**	**Resolution in range**	**Resolution in azimuth**	
			SLC	**ML**
X	vv	2.0 m	0.6 m	1.5 m
C	vv	2.0 m	0.6 m	1.5 m
L	vv, hh, hv, vh	2.0 m	0.8 m	2.0 m
P	vv, hh, hv, vh	4.0 m	1.6 m	4.0 m

Table 2. Characteristics of SAR data

Multi-spectral data were collected at very low altitude (330 m to get a high spatial resolution) in 12 different channels, ranging from visible blue to thermal infrared, with the

Daedalus scanner of DLR. Table 3. summarizes the characteristics of these multi-spectral data.

Channel Number	Spectral range (μm)	Wavelength of maximum sensitivity (μm)	Resolution
1	0.41-0.46	0.44	0.8 - 1.0 m
2	0.44-0.53	0.51	
3	0.51-0.62	0.58	
4	0.58-0.65	0.61	
5	0.61-0.72	0.65	
6	0.67-0.80	0.73	
7	0.73-1.00	0.83	
8	0.85-1.10	0.95	
9	1.45-1.82	1.71	
10	1.95-2.42	2.20	
11	8.20-14.0	10.00	
12	8.20-14.0	10.00	

Table 3. Characteristics of multi-spectral data

DLR also provided the SMART teams with a complete set of RMK photographic aerial views recorded with a coloured infrared film at a resolution of 3 cm. This latter data set, which is not geo-coded and far too large to be processed, has only been used as evidence to control the good working of processing tools and for qualitative interpretation by photo-interpreters. In the latter case, RMK images were registered manually with SAR and multi-spectral data. Finally, geo-coded KVR-1000 black-and-white satellite images recorded before the war in Croatia, with a resolution of 2 m, have been purchased in order to assess the changes in the landscape due to the war. Table 4. summarizes their characteristics.

Site	Date of record	Resolution	Type
Glinska Poljana	May 13, 1992	2.0 m	Panchromatic
Pristeg	May 13, 1992		
Ceretinci	June 04, 1988		

Table 4. Characteristics of KVR-1000 data

5. Image Processing Tools Concept

On basis of field campaigns and discussions with mine action specialists of CROMAC, it clearly appeared that the first step to achieve was to set up a list of features (called indicators) to look for in the data, based on what could be seen in the data and what could be related to the absence or presence of mines or minefields.

Indicator of mine absence	Indicator of mine presence	Data	Methods and Tools
Cultivated fields		MS	Classification
Asphalted roads		MS, SAR	Classification and detection
Infrastructures In use		MS, SAR	Classification and detection
	Trenches and man-made embankments	MS, SAR, RMK	Detection of linear features and interactive processing
	Bunkers	RMK	Interactive processing
	Concealed paths to trenches or bunkers	RMK	Interactive processing
	Shores of rivers	MS	Classification and detection
	River banks, shallow rivers or creek	RMK	Interactive processing
	Bridges (destroyed bridges included)	MS, RMK	Detection of linear features and interactive processing
	Tracks no longer in use	MS, KVR, RMK	Detection of linear features and interactive processing
	Agricultural areas no longer in use	MS, KVR	Classification and change detection
	Crossroads, especially with no longer used tracks	MS, KVR	Detection of linear features
	Irrigation/drainage	MS, SAR	Detection of linear features
	Edges of forests	KVR	Classification
	Hedges (defensive lines)	SAR	SAR specific detector
	Power supply poles	SAR	SAR specific detector
	Soft edges of hardtop roads	MS, SAR	Classification and detection
	Tank and canon holes	RMK	Interactive processing
	Mine accidents and Incidents	MAGIS	
	Minefield records	MAGIS	+ Analysis of confidence
	Confrontation zones	MAGIS	+ Conflict history reconstruction
	Hilltops and elevated Plateaus	DEM	Dedicated tool
	Dominant slopes and heights	RMK	Interactive processing
	Houses used as rooms, ammunitions stores, HQs, bunkers	Fieldwork	Interactive processing
	Damaged or destroyed houses	RMK	Interactive processing

Table 5. Indicators with corresponding data and processing tools

Obviously, indicators of absence of mine are the most important for helping to decide if a mine-safe area is actually mine-safe. Unfortunately, these indicators are not numerous. Although a key indicator of mine absence seems to be the cultivated fields, most of indicators available are indicators of mine presence. Therefore, SMART has two uses: (i)

area reduction as such - by detecting indicators of mine absence -, and (ii) suspicion reinforcement - by detecting indicators of mine presence (Yvinec, 2005).
The next step consists in developing methods and tools to detect these indicators. The developed methods and tools are based on two approaches: (i) anomaly detection (detecting specific objects in the data) and (ii) classification, i.e. assigning each pixel (pixel-based classification) or region (segment-based classification) to a specific land use class. Table 5. summarizes the list of indicators with the corresponding tools developed in SMART (MS means multi-spectral, MAGIS mine action GIS and KVR KVR-1000 satellite images). If 'Methods and tools' are called ``interactive processing", it means that the resolution of the multi-spectral and SAR data is not sufficient and that other means have been added as the photo-interpretation by image analysts of manually registered RMK high-resolution aerial views, recorded originally on films (coloured infrared) with a resolution of 3 cm and digitised on CD-ROM with a resolution of 10 cm.
The last step fuses the information produced by anomaly detectors and classifiers, considered as experts in a framework of belief functions or in a fuzzy approach, and builds the so-called risk maps as a probability map of mine presence (or mine absence) given the context.

6. Pre-processing

The pre-processing tasks consist in registering and geo-coding the available data as well as restoring the SAR images. The latter operation is necessary to reduce the speckle existing in SAR images. Appearing as a random granular pattern, speckle seriously degrades the image quality and hampers the subsequent pattern recognition processing.

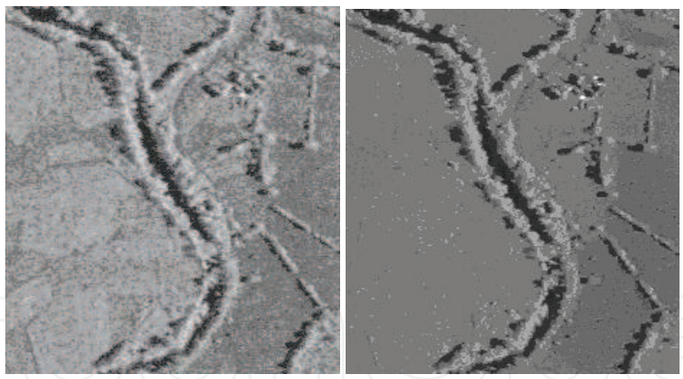

Fig. 2. Speckle reduction in SAR images.

The restoration process is based on the non-decimated wavelet transform. Each wavelet coefficient is multiplied by a given shrinkage factor (soft threshold), which is a function of the magnitude of the coefficient. In contrast with other methods, the algorithm used achieves a *soft* spatial adaptation, from the homogeneous to the highly heterogeneous areas.
The wavelet coefficients are not filtered in different regions according to different rules, but a unique shrinkage function is applied, that accounts for local statistics of the wavelet coefficients, and automatically adapts to the local spatial activity in the image (Pizurica et al, 1999; Duskunovic et al, 2000). Figure 2. gives an example of speckle reduction using this method.

7. Anomaly Detection

7.1. Bushes/Hedges, Trees, Water and Radar Shadow

Hedges growing on the border of agricultural fields are often used as defensive lines, protected by mines and are therefore good candidates of mine presence. In multi-spectral data, hedges and trees look very similar as only the top of the vegetation, the leaves, is seen. Radar waves penetration depends on the wavelength. While X-band waves (λ=3cm) are reflected mostly by the top of the vegetation (a few centimetres), L-band waves (λ=24cm) penetrates deeper into the vegetation structure and gets reflected into the volume of the vegetation. For larger wavelengths (λ =67cm for the P-band), the vegetation volume becomes invisible and the waves undergo double reflections at the ground and the trunk of trees. Because of this backscattering process, trees are clearly visible in the P-band thanks to double reflections between the trunk and the ground while bushes and hedges, not visible in the P-band, provoke volume reflections in the L-band, and the combined use of L- and P-band SAR data allows to distinguish efficiently trees from bushes and hedges. The cross-polarized L-band data[3] L_{xx} is best sensitive to backscattering in the vegetation volume while co-polarized P-band data (e.g. P_{hh}) is best sensitive to double reflections on the horizontal ground and the vertical trunk.

For a better separation of both targets from other objects additional parameters are used: the X_{vv} and P_{xx} channels[4], the 4th channel of the multi-spectral sensor, and the ratios P_{xx}/X_{vv} and P_{xx}/X_{hh}. Figure 3. gives an example of detected bushes and trees, using a composite image where red is P_{hh}, green L_{xx} and blue X_{vv} (Keller et al, 2004).

An area is classified as water if the backscattering is very low in the X_{vv} and L_{vv} channels (because of the specular reflection of very smooth areas), if the thermal infrared channel response of the multi-spectral sensor is very low (because of the low emission of cold objects), if the 4th channel response of the multi-spectral sensor is neither very dark nor very bright and if the area fulfils some size conditions.

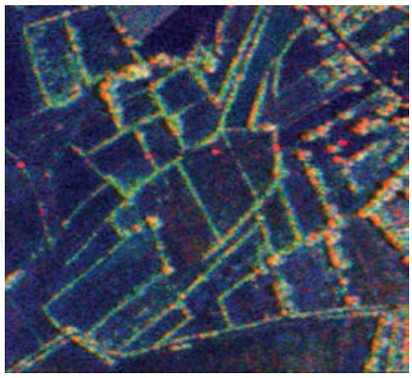

Fig. 3. Detection of hedges (green), trees (light red) and power line poles (dark red) from SAR data. Image courtesy of DLR

[3] For a monostatic configuration $L_{xx} = \frac{L_{vh}}{2} + \frac{L_{hv}}{2}$

[4] For a monostatic configuration $P_{xx} = \frac{P_{vh}}{2} + \frac{P_{hv}}{2}$

7.2. Power Lines

Power lines as important infrastructure are often considered as strategic targets protected with mines. Detecting automatically power lines can prove much more cost effective than extracting them manually on old and inaccurate maps.

Usually, in SAR images, power line poles induce strong double bounce reflections between the pole foot and the ground in the P-band, independent of the sensor flight direction. The absence of volume scattering distinguishes them from the vegetation (tree crowns) and makes easier discriminating between poles and tree trunks. Further, power line poles are too small to be detected using the multi-spectral data and only SAR data are used in the algorithm – a simple threshold operation (see poles in dark red on the image of Figure 3.).

In order to reduce the number of false alarms and to find power lines considered as an alignment of poles, a Hough transform applied on all detections in the image and makes for finding the aligned objects that with high probability belong to a power line.

7.3. Hilltop Detection

The detector allows the user to create contours and to determine an area where the altitude is higher than or equal to a given altitude. Obviously, this operation is performed using a DEM provided by the user if it exists (as it is the case in Croatia) or computed from interferometric SAR data.

7.4. Road and Abandoned Road Detection

7.4.1. Bright Line Detector in Multi-spectral Images

Detecting roads and paths on multi-spectral images involves detecting bright lines in single channels. A line is characterized by an edge at both sides of it. The gradient is positive at one side of the line and negative at the other side (anti-parallel gradients). This principle is used in line detection.

After applying a gradient operator on the image, the line response image consists of the detected anti-parallel gradients. Next, suppressing recursively the non-maxima of the line responses perpendicularly to each line results in a line strength image.

After breaking possible squares (clusters of four adjacent pixels), to convert the detected lines into vector objects, a minimum line strength is set to start each line object and to continue the line following.

To suppress false targets, the line candidates are filtered based on the grey-value of their underlying pixels, in order to secure sufficient absolute line brightness, and the candidates with a too small length are rejected.

All channels, in which roads appear as bright lines (i.e. channels 2, 3, 4, 9 and 10), are selected and a new image is made with in each of its pixel the maximum grey-value of the corresponding pixels of the selected channels. Finally, the algorithm just described is applied to this new image.

The previous method applies also to dark edges after obvious adjustment.

7.4.2 Multivariate Edge/Line Detector in SAR Images

The presence of speckle makes pixel-wise methods using a simple filtering mask inappropriate for edge detection in SAR images. The solution that is commonly adopted is

to take into account larger neighbourhoods of each pixel for deciding whether an edge passes through that pixel.
For deciding whether a vertical edge passes through pixel P in the images (see Figure 6. (a)), two rectangles are constructed around the point P and statistics are calculated in both rectangles. If the statistics differ, an edge passes; otherwise, there is no vertical edge. The test is repeated in every pixel for a given number of orientations of the set of scanning rectangles and the final edge strength is the maximum of the statistics differences for all orientations. The orientation corresponding to that maximum is the edge direction in the point.
The user can choose between different statistical tests (e.g. Hottelings, Levene, Student or Median tests) for comparing the statistics inside the scanning rectangles. For multi-channel data techniques, multivariate statistical hypothesis tests are used. For single channel SAR data a Touzi ratio detector[5] is implemented (Touzi et al, 1988). A few other methods are also possible (Borghys et al, 2002).

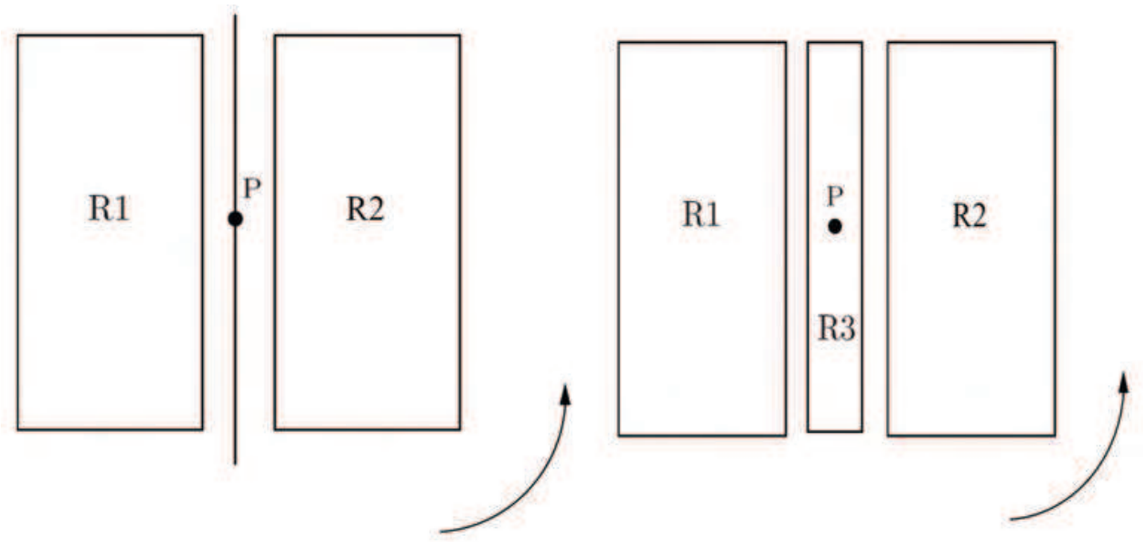

Fig. 6. (a) Multivariate edge detector. (b) Multivariate line detector.

For deciding whether a line passes through pixel P in the images (see Figure 6. (b)), three rectangles are used. The middle one is centred on the current point P and is narrower than the two others. In order to detect whether a line in a given orientation passes through point P, the statistics of the two outer rectangles are compared with those of the middle one. The response of the detector is the response corresponding to the smallest difference in statistics. This allows avoiding false alarms due to (single) edges. The width of the central rectangle is chosen such that it corresponds approximately to the possible widths of the lines (e.g. roads) to be detected.

[5] The Touzi edge detector is based on the ratio of averages in intensity images. The edge detector response between rectangle i and j is defined as $F_{R_iR_j} = 1 - \min\left(\frac{\mu_i}{\mu_j}, \frac{\mu_j}{\mu_i}\right)$

In SAR images it is often possible to predict whether a given object will appear as a bright or a dark line. Roads for instance will almost always appear as dark lines, because their surface is very smooth compared to the wavelength of the radar and only induces single reflections. In this case an extra condition can be applied in the line detection algorithm. The condition is based on a comparison of the average image intensity of the centre rectangle with the one found in the two outer rectangles. The user can choose between different tests for comparing the statistics inside the scanning rectangles.
For multi-channel log-intensity SAR data or multi-spectral data, a multivariate statistical hypothesis test of Hotellings is used. For single channel log-intensity SAR data, either a Student test (also valid for multi-spectral data) or a Touzi ratio detector (only for SAR data) can be performed.
All tests are applied after speckle reduction, either on the slant or the geo-coded SAR images. The best results are obtained after speckle reduction on the geo-coded log-intensity images, using the Hotellings test applied on all polarizations (or all bands in multi-spectral) at the same time. Although this gives the best results, applying the Student test to a single polarization is a lot faster. An example of line detection in a full polarimetric SAR image is given in Figure 7.

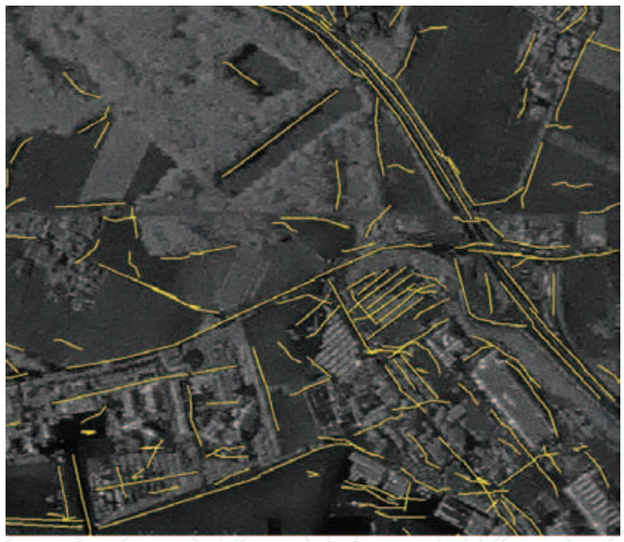

Fig. 7. Detection of lines in a full polarimetric L-band SAR image.

7.4.3 Road Tracker

The tool ``road tracker'' is used to follow a linear feature from an original point given by the user. As SAR data are subject to speckle, this tool is only applied on multi-spectral data. In an initialisation phase, the input image is smoothed using a Gaussian filter, the gradient and the Hessian of the smoothed image are computed at each pixel and for each pixel, the eigenvectors and eigenvalues of the Hessian are computed and the eigenvector associated to the largest eigenvalues is kept (if the pixel lies on a linear feature, this eigenvector is normal to the direction of the linear feature).

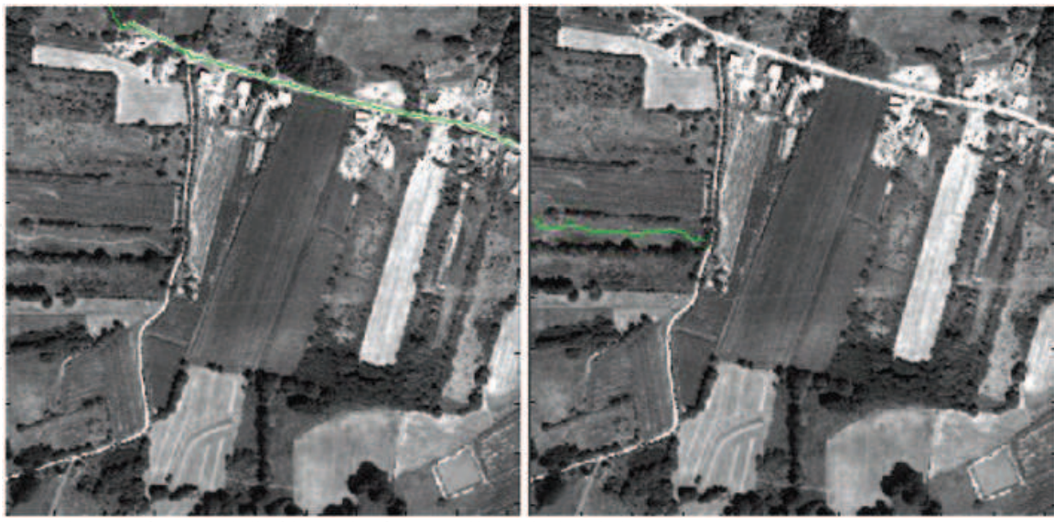

Fig. 4. Tracking of a road (left) and of a small path (right)

In a production phase, the starting point given by the user is improved by trying to move it closer to the middle of the linear feature. Therefore, a Principal Component Analysis (PCA) optimises the direction of the linear feature computed during the initialisation phase. Then, in the direction normal to the direction of the linear feature and in a surrounding window, the pixel with the smallest gradient (the new location of the starting point) is determined. A tracking algorithm is used in the best (from previous step) direction and its opposite. The tracking algorithm is based on a Kalman filter to correct and predict the next point. Figure 4. gives two examples of tracking results in green.

7.4.4 Abandoned Road Detection

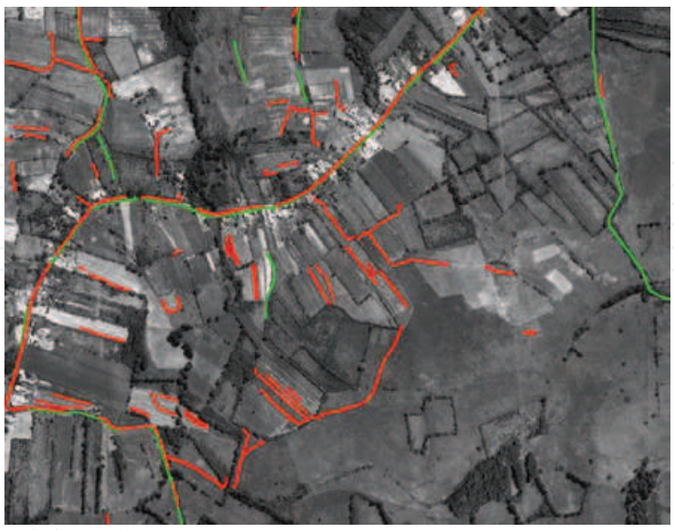

Fig. 5. Abandoned road detection

The methods described above can be used to detect changes in order to find abandoned roads. These methods are respectively applied to a pre-conflict panchromatic satellite image (KVR image) and a post-conflict airborne multi-spectral image (acquired with the Daedalus line scanner). For the multi-spectral image, the method is applied on three of the bands on which the roads appear as bright lines. The detection results are fused using a "AND" operator. Figure 5. shows the final result superimposed on a panchromatic Daedalus image, in red the detection on the Daedalus images, in green on the KVR image. Candidate abandoned roads are the lines which only appear in green. An interactive processing on the RMK images allows reducing the number of false candidates.

8 Feature Extraction

8.1. Texture Generation with a Gabor Filter Bank

Convolving an image (e.g. a channel of the multi-spectral images) with a bank of Gabor filters produces texture images. Each convolution with a specific filter from the bank produces a specific texture image. These texture images can be used as additional input images in the classification process to improve the detection of classes with specific textures. The Gabor filter bank consists of the following centred filters:

$$G(x, y, k_x, k_y) = e^{-\frac{x^2+y^2}{\sigma}} . e^{j(k_x x + k_y y)} \tag{3}$$

where x, y, k_x and k_y are respectively the spatial coordinates and the spatial frequencies.

Two simplifications are introduced to compute the convolution: (i) the Short Time Fourier Transform is used to compute the effect of the complex exponential and (ii) the Gaussian is approximated with a binomial window (Lacroix et al, 2005). A set of feature images is obtained by convolving the input image with each filter and by computing a local energy (the squared module of the result) in each pixel.

8.2. Polarimetric SAR Feature Extraction

8.2.1. Pauli Decomposition

The SAR complex backscattering coefficients (module and phase) are represented in each pixel by the backscattering or Sinclair matrix S:

$$S = \begin{bmatrix} S_{vv} & S_{vh} \\ S_{hv} & S_{hh} \end{bmatrix} \tag{4}$$

where, in the considered pixel, S_{xy} stands for the backscattering coefficient, which corresponds to a wave sent under polarization x and received under polarization y, x and y being h or v, respectively horizontal and vertical polarizations. The Pauli decomposition consists in the construction of the Pauli target vector **k** and the 3×3 coherence matrix T, given by (Cloude & Pottier, 1996):

$$\mathbf{k}^T = \frac{1}{\sqrt{2}} \left[(S_{hh} + S_{vv}) \quad (S_{hh} - S_{vv}) \quad 2.S_{hv} \right] \tag{5}$$

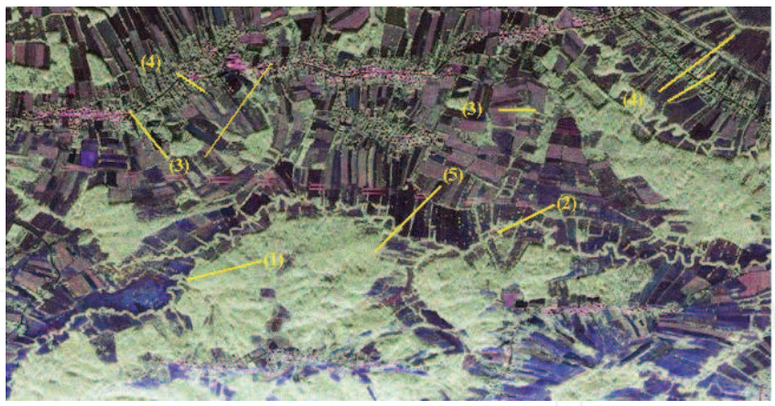

Fig. 8. Pauli decomposition in composite colours: (1) and (2) odd bounces in blue, (3) double bounces in red (4) double bounce at 45° w.r.t. the flight direction and (5) volume scattering in green. Image courtesy of DLR

where the superscript (T) stands for transpose, and

$$T = \mathbf{k}.\mathbf{k}^{*} \tag{6}$$

where the superscript (*) stands for transpose conjugate. The diagonal terms of (6), given by $|S_{hh}+S_{vv}|^2$, $|S_{hh}-S_{vv}|^2$ and $2.|S_{hv}|^2$ are close related to physical and geometrical properties of the scattering mechanism. The first one corresponds to odd bounce scattering (typically rough surfaces), the second one to double bounce scattering (typically in urban areas) and the third one to volume scattering (typically vegetation and forests). Figure 8. gives an example of Pauli decomposition in the region of Blingskikut.

8.2.2. Polarimetric Decomposition and Polarimetric Features

In 1997, S.R. Cloude and E. Pottier have developed a method that is free of the physical constraints imposed by assumptions related to a particular underlying statistical distribution (Cloude & Pottier, 1997). They derive important features as the entropy H, the anisotropy A and the angle α.

Let us consider an estimate $\overline{T}$ of the coherence matrix T, representing the averaged contribution of a distributed target over n pixels and given by:

$$\overline{T} = \frac{1}{n}\sum_{1}^{n} \mathbf{k}_i.\mathbf{k}_i^{*} \tag{7}$$

with eigenvalues λ_1, λ_2 and λ_3 of $\overline{T}$, ordered by decreasing value, as well as the corresponding orthonormal eigenvectors $\mathbf{u}_i$ (i=1…3), columns of the following 3×3 parametric unitary matrix:

$$e^{j\varphi_1}.\begin{bmatrix} \cos\alpha_1 & \cos\alpha_2.e^{j\varphi_2} & \cos\alpha_3.e^{j\varphi_3} \\ \sin\alpha_1.\cos\beta_1.e^{j\delta_1} & \sin\alpha_2.\cos\beta_2.e^{j(\delta_2+\varphi_2)} & \sin\alpha_3.\cos\beta_3.e^{j(\delta_3+\varphi_3)} \\ \sin\alpha_1.\sin\beta_1.e^{j\gamma_1} & \sin\alpha_2.\sin\beta_2.e^{j(\gamma_2+\varphi_2)} & \sin\alpha_3.\sin\beta_3.e^{j(\gamma_3+\varphi_3)} \end{bmatrix} \tag{8}$$

$\overline{T}$ may be rewritten as:

$$\overline{T} = \sum_{i=1}^{3} \lambda_i.\mathbf{u}_i.\mathbf{u}_i^{*} \tag{9}$$

where the eigenvalues λ_i represent statistical weights of three normalized targets $\mathbf{u}_i.\mathbf{u}_i^*$ (i=1 … 3).
The entropy H, or degree of randomness, is defined by

$$H = -\sum_{i=1}^{3} P_i.\log_3(P_i) \tag{10}$$

where the P_i's are probabilities estimated from the eigenvalues of $\overline{T}$:

$$P_i = \frac{\lambda_i}{\sum_{j=1}^{3} \lambda_j} \tag{11}$$

The entropy shows to which extent a target is depolarizing the incident waves. If H is close to zero, the target is weakly depolarizing ($\lambda_2 = \lambda_3 = 0$) and the polarization information is high. If H is close to one, the target is depolarizing the incident waves and the polarization information becomes zero and the target scattering is a random noise process. An object with a strong backscattering mechanism, e.g. a corner reflector (three reflections) or a wall (two reflections) will only show one scattering mechanism that will dominate all others, as the surface backscattering from the surrounding ground, and will have a very low entropy. A forests, because of the multiple reflections in the crown of the trees, will show a backscattering mechanism with polarization characteristics that are less and less related to the polarization of the incoming waves. All extracted scattering mechanisms will have a similar strength (the same probabilities P_i), and the entropy will be close to one.
The anisotropy A is defined as:

$$A = \frac{\lambda_2 - \lambda_3}{\lambda_2 + \lambda_3} \tag{12}$$

Most structures of the SAR intensity image are not longer visible in an anisotropy image, as λ_1, which contains the information of the most important scattering mechanism, does not appear in the latter expression.
Nevertheless, structures, invisible in other data sets, may appear. Anisotropy should never been used without considering the entropy.

The angle α is defined as:

$$\alpha = P_1.\alpha_1 + P_2.\alpha_2 + P_3.\alpha_3 \tag{13}$$

where the α_i's are defined in the parametric unitary matrix built with the eigenvectors of $\overline{T}$. It is easy to show that angle α, built from the eigenvalues and the eigenvectors of $\overline{T}$ and taking its values between zero and $\frac{\pi}{2}$, is a measure for the scattering mechanism itself. α angles close to zero mean that the scattering consists only of an odd number of bounces (e.g. single bounce from the ground, or triple bounce from a corner reflector or from corners at houses). α angles close to $\frac{\pi}{2}$ correspond to double bounce scattering, while α angles close to $\frac{\pi}{4}$ correspond to volume scattering.
Further, it can be shown that the eigenvalues λ_i, thus the probabilities P_i, the entropy H and the anisotropy A, as well as α are all roll-invariant, that is these quantities are not

sensitive to changes of the antenna orientation angle around the radar line of sight. Figure 9. presents an example of image obtained with entropy H, angle α and backscattered intensity.

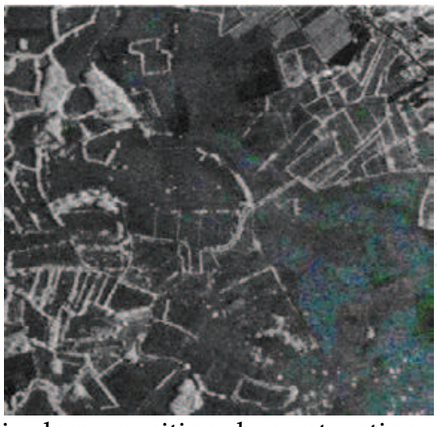

Fig. 9. Example of polarimetric decomposition: hue-saturation-value colour composite of respectively angle α, inverse entropy 1-H and backscattered intensity. Image courtesy of DLR

8.2.3. Interferometric Coherence

In order to define the polarimetric interferometric coherence, the polarimetric complex coherences first need to be defined. In this case, two polarimetric image sets (A and B) are analysed. Stacking the above-defined target vectors $\mathbf{k}_A$ and $\mathbf{k}_B$ of polarimetric image sets A and B respectively provides the new target vector $\mathbf{k}_6$:

$$\mathbf{k}_6 = \begin{bmatrix} \mathbf{k}_A \\ \mathbf{k}_B \end{bmatrix} \tag{14}$$

The 6×6 corresponding interferometric coherence matrix T_6 is estimated by $\overline{T}_6$ given by averaging over n pixels:

$$\overline{T}_6 = \frac{1}{n}\sum\nolimits_n \mathbf{k}_6.\mathbf{k}_6^{*} \tag{15}$$

or

$$\overline{T}_6 = \begin{bmatrix} \overline{T}_{AA} & \overline{\Omega}_{AB} \\ \overline{\Omega}_{AB}^{*} & \overline{T}_{BB} \end{bmatrix} \tag{16}$$

where $\overline{T}_{AA}$ and $\overline{T}_{BB}$ are the estimates of coherence matrices for the image sets A and B respectively, $\overline{\Omega}_{AB}$ is the 3×3 polarimetric cross-coherence matrix. From the elements of this latter matrix, the three polarimetric complex coherences (γ_1, γ_2 and γ_3) can be computed as follows:

$$\gamma_i = \frac{\overline{k}_{A_i}.\overline{k}_{B_i}^{*}}{\sqrt{\overline{k}_{A_i}.\overline{k}_{A_i}^{*}.\overline{k}_{B_i}.\overline{k}_{B_i}^{*}}} \tag{17}$$

where the $\overline{k}_{X_i}$ are the estimates of the corresponding component of $\mathbf{k}_X$, with X being A or B.

Coherence may be decomposed into multiplicative contributions including the backscattered signal-to-noise ratio, the spatial distribution of the illuminated scatterers, temporal variation between acquisitions and the polarization state (Papathanasiou, 2001). Figure 10. gives an example of an interferometric coherence image in composite colours (a low coherence is dark, a high coherence is bright).

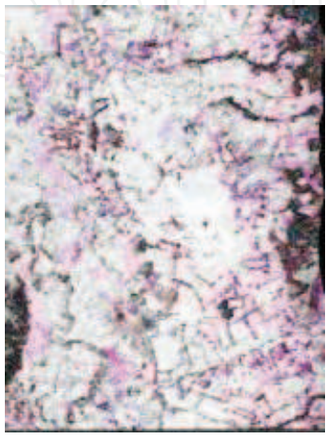

Fig. 10. Interferometric coherence image in composite colours: γ_1 $(\mathrm{hh_A} - \mathrm{hh_B})$ in red, γ_2 $(\mathrm{hv_A} - \mathrm{hv_B})$ in green and γ_3 $(\mathrm{vv_A} - \mathrm{vv_B})$ in blue. Image courtesy of DLR

9. Classification

9.1. Minimum Distance Classifier

This supervised and pixel-based classification method, applied on multi-spectral data assumes the availability of a training set with C known classes i in spectral band j with centres $c_{i,j}$ and standard deviation $\sigma_{i,j}$ in the feature space consisting of grey-values $p_j(m,n)$, where m and n are the pixel coordinates. Texture data may be added to the set of spectral bands. For each pixel, a minimum discounting distance $d(m,n)$ is computed as follows:

$$d(m,n) = \min_{i=1}^{C} \sqrt{\frac{1}{N} \sum_{j=1}^{N} \sigma_{i,j} \cdot (p_j(m,n) - c_{i,j})^2} \tag{18}$$

where N is the number of bands. If $d(m,n)$ is smaller than or equal to the pre-set maximum distance d_{max}, the resulting pixel value $r(m,n)$ is set to the number of the winning class. Otherwise, the pixel is considered as belonging to an unknown class and its value $r(m,n)$ is set to 255. Distance discounting per band and per class using the standard deviation $\sigma_{i,j}$ has been introduced in (18) so that the higher the deviation is, the wider (less precise) the corresponding distance is. At the same time, a confidence $t(m,n)$ image is computed, given for pixel (m,n) by:

$$t(m,n) = p_{max}.(1 - \frac{d(m,n)}{D_s}) \quad (19)$$

where p_{max} is the maximum grey-scale value (255), and D_s is the maximum distance for class s, with $s = r(m,n)$.

9.2. Classifier Based on Belief Functions

This tool classifies each band on a pixel basis and fuses the results through the belief functions framework. The theory of belief functions (Shafer, 1976) allows saying explicitly that two hypotheses cannot be distinguished. Then the two hypotheses can be merged into what is called a focal element, here a set of classes.

This classifier assigns a focal element to each pixel based on knowledge on how likely a pixel belongs to that focal element given its pixel values in the different channels. This likelihood is measured by what is called a mass.

The theory of belief functions does not require any specific method to compute the masses, provided the masses follow certain rules. For instance the higher the mass, the more likely the belonging to the focal element. The masses must be between 0 and 1. For a given pixel value and a given channel, the sum of all masses over all focal elements equals one.

In order to perform the classification, the classifier must take into consideration all the hypotheses and the evidence supporting them. A hypothesis is that the pixel belongs to a given focal elements. The belief functions framework offers several possible rules for this final decision.

The classifier can choose the hypothesis that is the most supported by evidence. This is called the maximum of belief. In order to avoid the cases where the chosen focal element consists of several classes leading to an ambiguous classification, it is possible to restrict the choice of focal elements to singletons, i.e. focal elements consisting of one class.

The classifier can also choose the hypothesis that is the less in contradiction with the available evidence. This is called the maximum of plausibility. Again the choice may be restricted to singletons in order to have an unambiguous classification.

A compromise between the maximum of belief and the maximum of plausibility can be found with the pignistic probabilities obtained by reallocating the mass of every non-singleton focal element uniformly over its members. Restricting the choice to singletons can be done here too.

In SMART, only the maximum of belief with singletons was computed and generated in order to simplify the use of the tool.

The belief functions framework is used to perform data fusion of the points of views of different experts. Here each band is an expert and the masses given as input are the expertise of each expert concerning the possible classification of each band.

The algorithm combines this information according to the belief functions model and computes the evidence for each hypothesis. More information on this classification method can be found in Chapter 4.

9.3. SAR Supervised Classifier with Multiple Logistic Regression

The supervised classification based on the multinomial logistic regression is a pixel-based method where all classes j are considered at the same time (Borghys et al, 2004a). The last

class j^* is the so-called baseline class. As all classes are considered at the same time, the sum of the conditional probabilities of the different classes equals one in each pixel. For the non-baseline classes, the multinomial logistic function is given by:

$$p_{m,n}(c = j / \mathbf{F}) = \frac{e^{\beta_{0j} + \sum_i F_i(m,n)\beta_{ij}}}{1 + \sum_{k \neq j^*} e^{\beta_{0k} + \sum_i F_i(m,n)\beta_{ik}}} \quad (20)$$

with $c \neq j^*$ and where the sum is over all classes. For the baseline class j^*, it is given by

$$p_{m,n}(c = j^* / \mathbf{F}) = \frac{1}{1 + \sum_{k \neq j^*} e^{\beta_{0k} + \sum_i F_i(m,n)\beta_{ik}}} \quad (21)$$

Note that in case of dichotomous problems where a target class has to be distinguished from the background, the multinomial logistic regression is reduced to the simple logistic regression, which simplifies equations (20) and (21). Because of the complexity of the classes for the Glinska-Poljana test site, it was decided to develop a hierarchical, tree-based, classification (Borghys et al, 2004b). Figure 11. presents an overview of the classification tree used in SMART. At the first level, a logistic regression separates the group of "forests and hedges" from all other classes. Forests and hedges are separated from each other using again a logistic regression. Next, the other classes are separated with a multinomial regression. In this way, at each level, the full discriminative power of the features **F** is focused on a sub-problem of the classification.

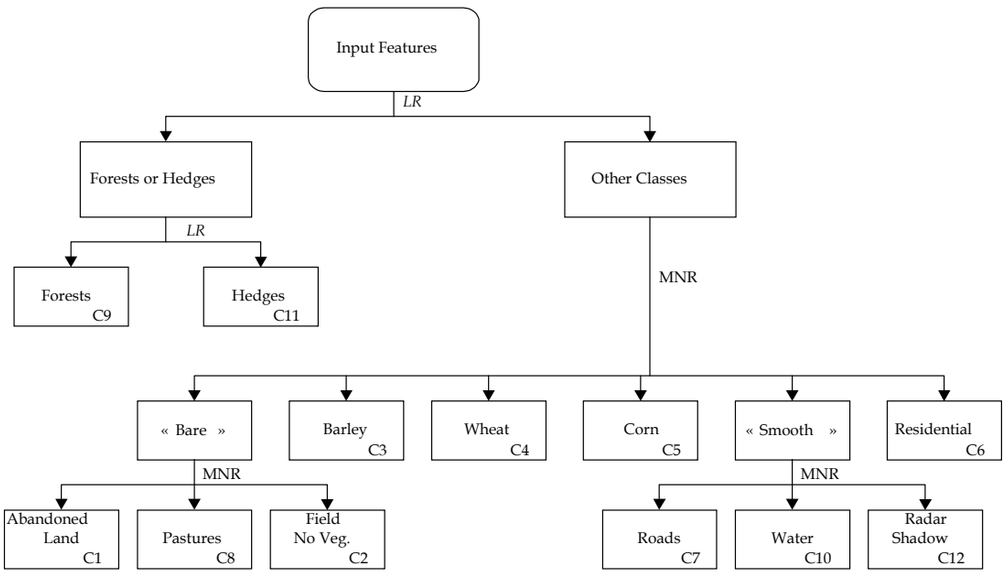

Fig. 11. SAR data classification tree in Glinska-Poljana.

The logistic (LR) and multinomial (MNR) regressions are applied to all pixels of the SAR image set, according to the tree described in Figure 11., and a "detection image" $p_{m,n}(c = j^* / \mathbf{F})$ for each class j (from C1 to C12) is obtained. The pixels in a detection image

corresponding to a given class represent the conditional probability that the pixel belongs to that class given all features **F**. The detection images are combined in a classification process using majority voting, i.e. the class with the highest sum of conditional probabilities in a neighbourhood of each pixel is assigned to that pixel. This majority voting has to be performed at each level of the tree and the derived decision is used as a mask for the classification at the next level.

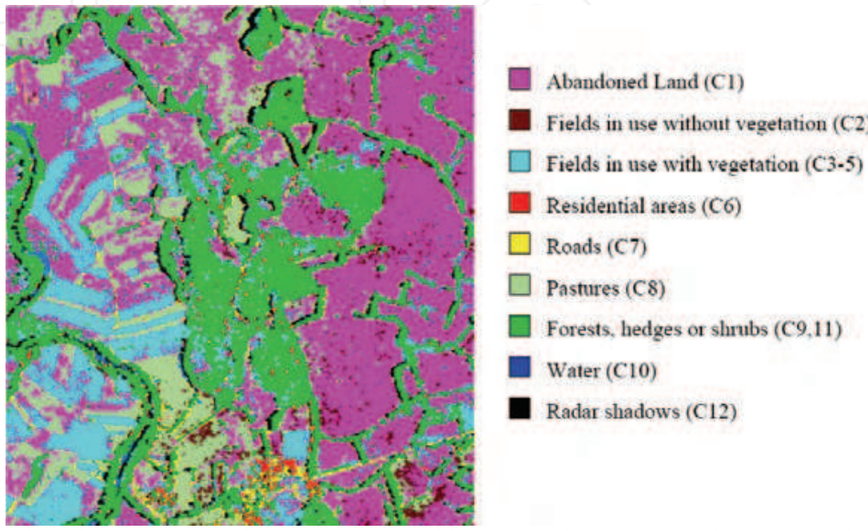

Fig. 12. SAR data hierarchical classification in Glinska-Poljana, using logistic and multinomial logistic regressions

Although this method gives conditional probabilities at each level, it is not possible to compare probabilities obtained at different tree levels. Figure 12. gives the results of the classification on the region of Glinska-Poljana.

9.4. Region-based Classifier

Region-based classification does not classify single pixels, but image objects extracted in a prior segmentation phase. A segmentation divides an image into homogeneous regions of contiguous pixels, used as building blocks and information carriers for subsequent classification. Beyond spectral information, regions contain additional attributes for classification, as shape, texture, and a set of relational/contextual features. In region growing procedures, the process starts with one-pixel objects, and uses local properties to create regions. Adjacent objects with the smallest heterogeneity growth are merged. To perform a supervised classification, features are defined and their values are computed for each region of a training set and a validation set, in order to train and validate the feature space, in which class centres and specific properties are recorded. In SMART, a supervised region-based fuzzy classification method has been used (Landsberg et al, 2006). The classification itself of the test data is performed in the feature space using fuzzy logic. A fuzzy classification method assigns an image object (region) to one class and defines at the same time the membership of this object to all considered classes. Class properties are defined using a fuzzy nearest neighbour algorithm or by combining fuzzy sets of object features, defined by membership functions.

Fig. 13. Supervised fuzzy region-based classification results in Ceretinci

It has been decided to work on land use rather than on land cover, as it is mandatory in the context of mine action to discriminate used land from unused land. This imperative made the classification process a complex issue since internal variability is higher in land use than in land cover.

The feature set includes the mean values, standard deviations and shape features for each radiometric multi-spectral channel as well as for pseudo-channels created to increase the number of features available. These pseudo-channels include a NDVI channel produced from channels 7 and 5 of the multi-spectral sensor, two PCA channels made respectively with the largest and the second largest components of a Principal Component Analysis performed on all multi-spectral channels and 12 channels made with the 11 Haralick texture parameters (Haralick et al, 1973) and a second order statistics, all 12 computed from the two previous PCA channels. A subjective interactive method gave the best results to select the most discriminant features.

The classification process produces two images for each class. A first one gives the membership value of each region to that class and a second one the regions classified in that class. Figure 13. gives the classification results for an area in Ceretinci.

10. Change Detection

As far as change detection is concerned the challenge was to develop a new method that makes it possible to use data from different sensor types. A region-based fuzzy post-classification change detection method, similar to the classification method described in the previous Section, was developed in order to detect the land use changes in agricultural areas, and more particularly plots that were cultivated before the war and neglected after the war. This method has assets over traditional post-classification change detection methods. First, it uses a combination of historical Very High Resolution panchromatic (black and white) satellite data and of recent Very High Resolution multi-spectral aerial data. This possibility to use data from different sensor types for change detection opens new

perspectives since historical VHR data are available mostly in the panchromatic mode. Second, it is based on a fuzzy approach: memberships to land use classes are used to map changes, but also to give a degree of confidence in the change detection results.

11. Data Fusion

The work on fusion was based on general considerations and theoretical work on possible fusion schemes, on main numerical methods as well as on the analysis of the characteristics of available data and pieces of knowledge. Based on this preliminary work, generic fusion tools were designed and implemented, mainly in the framework of belief function theory. In SMART, fusion aims at combining results provided by experts, here classifiers and anomaly detectors.

Numerous variants of belief function theories were designed and tested. Two of them appear as very promising, since they provide with good results and are very easy to adapt to other problems. The first one considers each classifier and anomaly detector as one information source. The classes of interest are the focal elements. The masses are discounted by a factor learned from the trace of the confusion matrix obtained for this classifier on the training regions and a mass is assigned to the whole set of discernment. The second one considers each class output by each classifier or anomaly detector as an information source. Focal elements for each source are derived from the line of the confusion matrix for this class, in order to account for possible confusions with other classes.

A simple fuzzy method provides with good results too, is faster, but remains somewhat specific. This method is based on the choice of the best classifiers or anomaly detectors for each class before combining them with a maximum operator (possibly with some weights). The decision is made according to a maximum rule. For each class, the best classifiers or anomaly detectors are those with the best diagonal element corresponding to this class in their confusion matrix.

A strong feature of the proposed methods is that additional knowledge can be included easily during the fusion and in the decision result. This feature allows for better results on the classes that are the most important ones for risk map construction, and for which knowledge is simple and straightforward (sure detection of roads, change detection, etc.).

A final spatial regularization step, based on the segmentation into homogeneous regions discussed in section 9.4, allows for obtaining less noisy classification results.

The overall results obtained at the end of this processing by all methods are better than those provided by each classifier or anomaly detector individually, and therefore constitute a useful input for risk map construction. The problem of fusion is discussed in more detail in Chapter 4.

12. Conclusions

This Chapter concentrates on the mine action technology problem and more specifically on the description of the processing algorithms used in the SMART project on area reduction. Nevertheless, the SMART approach has its limitations. The general knowledge used in SMART is strongly context-dependent. It has been currently derived from the study of three different test sites in Croatia chosen to be representative of South-East of Europe. In the case of another context a new field campaign is needed in order to derive and implement new

general rules. Before using SMART the list of indicators must be re-evaluated and adapted. For instance it has been noted that the assumption that a cultivated field is not mined, although quite valid in Croatia, may not apply in other countries such as South Africa or Colombia. It must also be checked if the indicators can be identified on the data and if the new list is enough to reduce the suspected areas.

13. Acknowledgements

The authors wish to thank all the researchers of the SMART and of the HUDEM / BEMAT[6] projects without whom it would have been impossible to write this chapter. More specifically, the authors would like to associate to this work the following research institutes and their key-personal who participated to SMART. The Scientific Council of CROMAC (Prof. Dr M. Bajic, Milan.Bajic@zg.htnet.hr and Prof. H. Gold, hrvoje.gold@fpz.hr), represented the end-users and was involved in the validation process. The "Ecole Nationale Supérieure des Télécommunications" (Prof. Dr Ir I. Bloch, Isabelle.Bloch@enst.fr), was very active in classification and data fusion. DLR - German Aerospace Centre (Prof. Dr H. Süss, Helmut.Suess@dlr.de and M. Keller) was responsible for data collection, preprocessing and SAR processing. TRASYS SPACE S.A. (Ir J. Willekens, Jacques.Willekens@trasys.be) has managed the project and its integration. The "Université Libre de Bruxelles / IGEAT" (Prof. Dr E. Wolff, ewolff@ulb.ac.be, S. Vanhuysse and F. Landsberg) was responsible for the field surveys, and efficiently contributed to classification, change detection and risk map design. Finally, the Royal Military School / SIC was responsible for the project technical management, and has been involved in data fusion (Dr Ir N. Milisavljević, Nada.Milisavljevic@rma.ac.be), classification and feature extraction (Dr D. Borghys, Dirk.Borghys@rma.ac.be).

14. References

M. Acheroy, "Mine action technologies: Problems and recommendations," Journal for Mine Action, vol. 7, no. 3, December 2003.

M. Acheroy, "Mine action: status of sensor technology for close-in and remote detection of antipersonnel mines", *Near Surface Geophysics*, vol. 5, pp. 43-56, 2007.

D. Borghys, V. Lacroix, and C. Perneel, "Edge and line detection in polarimetric SAR images," in International Conference on Pattern Recognition, Quebec, Canada, August 2002.

D. Borghys, C. Perneel, M. Acheroy, M. Keller, H. S¨uss, A. Pizurica, W. Philips, "Supervised Feature-based Classification of Multi-channel SAR Images Using Logistic Regression," in EUSAR2004 Conference, Ulm, Germany, May 2004.

D. Borghys, C. Perneel, Y. Yvinec, A. Pizurica, W. Philips, "Hierarchical Supervised Classification of Multi-channel SAR images," in 3rd International Workshop on Pattern Recognition in Remote Sensing PRRS'04. UK: Kingston University, Kingston upon Thames, August 2004.

[6] The Belgian project on humanitarian demining has been funded by the Belgian Ministry of Defence and the Belgian State Secretariat on Development Aid.

S.R. Cloude, E. Pottier, "A review of target decomposition theorems in radar polarimetry," IEEE Transaction on Geoscience and Remote Sensing, vol. 34, no. 2, pp. 498–518, March 1996.

S.R. Cloude, E. Pottier, "An entropy based classification scheme for land applications of polarimetric SAR," IEEE Transaction on Geoscience and Remote Sensing, vol. 35, no. 1, pp. 68–78, January 1997.

P. Druyts, Y. Yvinec, M. Acheroy, "Usefulness of semi-automatic tools for airborne minefield detection," in CLAWAR'98. Brussels, Belgium: BSMEE, November 1998, pp. 241–248.

I. Duskunovic, G. Stippel, A. Pizurica, W. Philips, and I. Lemahieu, "A New Restoration Method and its Application to Speckle Images,," in IEEE International Conf. on Image Proc. (ICIP 2000), Vancouver, BC, Canada, September 2000, pp. 273–276.

EODIS, "http://www.eodis.org/." SWEDEC EOD information system website.

EUDEM-2, "http://www.eudem.vub.ac.be/." Mine Action Technology website.

GICHD, "http://www.gichd.ch/." Geneva International Centre on Humanitarian Demining website.

R.M. Haralick, K. Shanmugan, I. Dinstein, "Textural features for image classification," IEEE Transaction on Systems, Man, and Cybernetics, vol. 3, no. 6, pp. 610–621, 1973.

ICBL, Landmine Monitor - Towards a Mine-Free World - Report 2005. USA: Human Right Watch, October 2005.

ITEP, "http://www.itep.ws/." Test & Evaluation of Mine Action Technologies.

JMU, "http://www.maic.jmu.edu/." USA: Website of the Mine Action Information Center at the James Madison University.

M. Keller, B. Dietrich, R. Mller, P. Reinartz and M. Datcu, "Report on DLR work in SMART," Tech. Rep., September 2004.

V. Lacroix, E. Wolff and M. Acheroy, "PARADIS: A Prototype for Assisting Rational Activities in humanitarian Demining using Images from Satellites," Journal for Mine Action, vol. 6, no. 1, May 2001.

V. Lacroix, M. Idrissa, A. Hincq, H. Bruynseels and O. Swartenbroekx, "Detecting Urbanization Changes Using SPOT5," Pattern Recognition Letters, to appear 2005.

F. Landsberg, S. VanHuysse, E. Wolff, "Fuzzy multi-temporal land-use analysis and mine clearance application," Photogrammetric Engineering and Remote Sensing, 2006.

Menard, Scott, "Applied logistic regression analysis," Sage Publications - Series: Quantitative Applications in the Social Sciences, no. 106.

N. Milisavljevi´c and I. Bloch, "Fusion of Anti-Personnel Mine Detection Sensors in Terms of Belief Functions, a Two-Level Approach," IEEE Trans. on Systems, Man and Cybernetics, Part B, 2002.

K.P. Papathanassiou, S.R. Cloude, "Single-baseline polarimetric SAR interferometry," IEEE Transaction on Geoscience and Remote Sensing, vol. 39, no. 6, pp. 2352–2363, November 2001.

A. Pizurica, W. Philips, I. Lemahieu and M. Acheroy, "Speckle Noise Reduction in GPR Images," in International Symposium on Pattern Recognition "In Memoriam Prof Pierre Devijver", Royal Military Academy. Brussels, Belgium: RMA, Februari 1999.

G. Schafer, A Mathematical Theory of Evidence. Princeton, New Jersey: Princeton University Press, 1976.

SMART consortium, "Smart final report," Tech. Rep., December 2004.

R. Touzi, A. Lopes, and P. Bousquet, "A statistical and geometrical edge detector for SAR images," in Proceedings of the IEEE-GRS Conference, vol. 26(6), November 1988, pp. 764–773.

Y. Yvinec, "A validated method to help area reduction in mine action with remote sensing data," in Proceedings of the IEEE ISPA-2005 Conference, Zagreb, Croatia, September 2005.

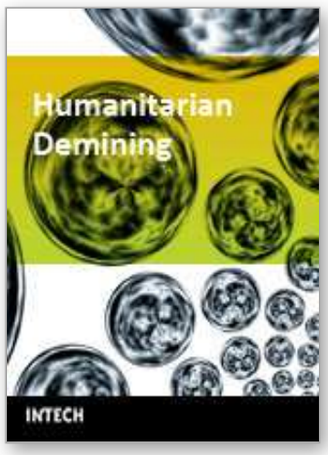

Humanitarian Demining

Edited by Maki K. Habib

ISBN 978-3-902613-11-0
Hard cover, 392 pages
Publisher I-Tech Education and Publishing
Published online 01, February, 2008
Published in print edition February, 2008

United Nation Department of Human Affairs (UNDHA) assesses that there are more than 100 million mines that are scattered across the world and pose significant hazards in more than 68 countries. The international Committee of the Red Cross (ICRC) estimates that the casualty rate from landmines currently exceeds 26,000 persons every year. It is estimated that more than 800 persons are killed and 1,200 maimed each month by landmines around the world. Humanitarian demining demands that all the landmines (especially AP mines) and ERW affecting the places where ordinary people live must be cleared, and their safety in areas that have been cleared must be guaranteed. Innovative solutions and technologies are required and hence this book is coming out to address and deal with the problems, difficulties, priorities, development of sensing and demining technologies and the technological and research challenges. This book reports on the state of the art research and development findings and results. The content of the book has been structured into three technical research sections with total of 16 chapters written by well recognized researchers in the field worldwide. The main topics of these three technical research sections are: Humanitarian Demining: the Technology and the Research Challenges (Chapters 1 and 2), Sensors and Detection Techniques for Humanitarian Demining (Chapters 3 to 8), and Robotics and Flexible Mechanisms for Humanitarian Demining respectively (Chapters 9 to 16).

INTECH
open science | open minds

InTech Europe
University Campus STeP Ri
Slavka Krautzeka 83/A
51000 Rijeka, Croatia
Phone: +385 (51) 770 447
Fax: +385 (51) 686 166

InTech China
Unit 405, Office Block, Hotel Equatorial Shanghai
No.65, Yan An Road (West), Shanghai, 200040, China
中国上海市延安西路65号上海国际贵都大饭店办公楼405单元
Phone: +86-21-62489820
Fax: +86-21-62489821

IntechOpen

IntechOpen